Crystal growth and ambient and high pressure study of the re-entrant superconductor $Tm_2Fe_3Si_5$

2008 J. Phys.: Condens. Matter 20 235243

(http://iopscience.iop.org/0953-8984/20/23/235243)

J. Phys.: Condens. Matter **20** (2008) 235243 (7pp) doi:10.1088/0953-8984/20/23/235243

Crystal growth and ambient and high pressure study of the re-entrant superconductor $Tm_2Fe_3Si_5$

Yogesh Singh[1] **and S Ramakrishnan**

Tata Institute of Fundamental Research, Mumbai-400005, India

Received 22 January 2008, in final form 7 April 2008
Published 13 May 2008
Online at stacks.iop.org/JPhysCM/20/235243

Abstract

$Tm_2Fe_3Si_5$ is known to undergo a transition to the superconducting state (at ambient or applied pressure depending on the sample) at a temperature T_{c1} ($\sim$1.8 K), and at a lower temperature T_N ($\approx$1 K) it undergoes a transition into a long range antiferromagnetically ordered state. Superconductivity is simultaneously destroyed and the sample re-enters the normal state at $T_{c2} = T_N$. The conditions reported in the literature for the observation of superconductivity in $Tm_2Fe_3Si_5$ are sample dependent, but it is now accepted that stoichiometric $Tm_2Fe_3Si_5$ superconducts only under pressure. Here we report single-crystal growth of stoichiometric $Tm_2Fe_3Si_5$ which does not superconduct at ambient pressure down to 100 mK. Measurements of the anisotropic static magnetic susceptibility $\chi(T)$ and isothermal magnetization $M(H)$, ac susceptibility $\chi_{ac}(T)$, electrical resistivity $\rho(T)$ and heat capacity $C(T)$ at ambient pressure and $\chi_{ac}(T)$ at high pressure are reported. The magnetic susceptibility along the c axis, $\chi_c(T)$, shows a curvature over the whole temperature range and does not follow the Curie–Weiss behavior, while the magnetic susceptibility along the a axis, $\chi_a(T)$, follows a Curie–Weiss behavior between 130 and 300 K with a Weiss temperature θ and an effective magnetic moment μ_{eff} which depend on the temperature range of the fit. The easy axis of magnetization is perpendicular to the c axis and $\chi_a/\chi_c = 3.2$ at 1.8 K. The ambient pressure $\chi_{ac}(T)$ and $C(T)$ measurements confirm bulk antiferromagnetic ordering at $T_N = 1.1$ K. The sharp drop in $\chi_{ac}(T)$ below the antiferromagnetic transition is suggestive of the existence of a spin gap. We observe superconductivity only under applied pressures $P \geqslant 2$ kbar. The temperature–pressure phase diagram showing the non-monotonic dependence of the superconducting transition temperature T_c on pressure P is presented.

1. Introduction

The series of compounds $R_2Fe_3Si_5$ (R = Sc, Y, Sm, and Gd–Lu) show interesting magnetic and superconducting properties [1–6]. Compounds of this series containing magnetic rare-earth elements Gd–Er show antiferromagnetic ordering of trivalent rare-earth moments [4, 5] and $Yb_2Fe_3Si_5$ has recently been shown to be a strongly correlated Kondo lattice system with a heavy Fermi liquid ground state surviving inside an antiferromagnetically ordered state [7]. The non-magnetic compounds with R = Sc, Y, and Lu show superconductivity at relatively high temperatures (T_c = 4.4, 1.8 and 6.2 K respectively) given the large Fe content [6]. Mössbauer measurements on $R_2Fe_3Si_5$ have shown that there is no moment on the Fe and it only contributes in building a large density of states at the Fermi energy [2, 8, 9]. The compound $Tm_2Fe_3Si_5$ is one of the most interesting in this series. It was shown to be the first re-entrant antiferromagnetic superconductor where superconductivity at $T_{c1} \sim 1.5$–1.8 K is destroyed by the onset of antiferromagnetism at $T_{c2} = T_N \sim 1\ K < T_{c1}$ [10–13]. $Tm_2Fe_3Si_5$ therefore is a unique system unlike other stoichiometric re-entrant superconductors which either become superconducting again at low temperature once the antiferromagnetic order is established (such as $HoNi_2B_2C$) [14] or become normal due to ferromagnetism in the first place ($ErRh_4B_4$) [15]. It is still not understood why the antiferromagnetic order among Tm^{3+} ions is a deterrent to superconductivity in $Tm_2Fe_3Si_5$ given

[1] Present address: Ames Laboratory and Department of Physics and Astronomy, Iowa State University, Ames, IA 50011, USA.

that earlier neutron scattering studies [13] could not find any ferromagnetic moment below T_N which could compete with the superconductivity.

Although there have been several studies on this material, there are varying reports about the onset of superconductivity in $Tm_2Fe_3Si_5$ with some groups reporting the onset of superconductivity below 1.8 K at ambient pressure [10, 11] while others observe superconductivity only under applied pressure [12, 13]. It has been shown in a recent study that the homogeneity range of $Tm_2Fe_3Si_5$ is small and that any internal pressure due to the off-stoichiometry and the presence of impurity phases can lead to varying values of T_{c1} [16]. That study also showed that stoichiometric $Tm_2Fe_3Si_5$ will superconduct only under pressure [16].

A detailed experimental investigation of the magnetic, thermal and electrical properties of stoichiometric $Tm_2Fe_3Si_5$ has not been reported before. In this work we report the growth of stoichiometric single-crystalline samples of $Tm_2Fe_3Si_5$ and their electrical resistivity ρ versus temperature T, static χ and ac magnetic susceptibility χ_{ac} versus T, magnetization M versus magnetic field H, and heat capacity C versus T at ambient pressure and χ_{ac} versus T at high pressure. Our data suggest valence fluctuations and/or the partial gapping of the Fermi surface below the antiferromagnetic ordering temperature as possible mechanisms for the destruction of superconductivity at low temperatures.

2. Experimental details

Single crystals of $Tm_2Fe_3Si_5$ were grown by a modified vertical Bridgman method. The purity of the rare-earth element Tm and the transition metal element Fe were 99.99% whereas the purity of Si was 99.999%. First, 5 g of a polycrystalline sample was prepared by arc-melting the constituent elements. The Fe and Si were taken in stoichiometric proportions and about 5% extra Tm over the stoichiometric amount was taken to compensate for any loss of Tm, due to its high vapor pressure, during the synthesis. The resulting tablet was remelted several times to promote homogeneity. The mass loss at this stage was negligible. This polycrystalline tablet was crushed into a fine powder and placed in an alumina crucible. This in turn is placed inside a tantalum container and sealed in an arc furnace under an ultrahigh purity argon atmosphere. The whole assembly is placed in a vertical tube furnace and slowly heated to 1450 °C in a dynamic Ar atmosphere and kept there for 4–6 h. The sample assembly is then pulled out of the furnace at a rate of 2–3 mm h^{-1}.

All measurements were performed on a single crystal of mass $m = 4.2$ mg. The temperature dependence of the magnetic susceptibility $\chi(T)$ and the isothermal magnetization $M(H)$ with the magnetic field along the a, b or c axes, was measured using the horizontal rotator option of a commercial SQUID magnetometer (MPMS5, Quantum Design). The resistivity $\rho(T)$ between 1.5 and 300 K was measured using an LR-700 ac resistance bridge by the four-probe method with contacts made with silver paste. The heat capacity $C(T)$ in zero field between 0.3 and 35 K was measured using a commercial PPMS (Quantum Design). The ambient pressure ac susceptibility $\chi_{ac}(T)$ between 0.1 and 4 K was measured at a frequency of 1 kHz, with an ac amplitude of 1 G, using an adiabatic demagnetization fridge (Cambridge Magnetic Refrigeration, Cambridge). The high pressure $\chi_{ac}(T)$ between 1.8 and 10 K were measured using the mutual induction option of the LR-700 ac resistance bridge. In this case the primary and the secondary coils, each of roughly 100 turns of 0.25 mm Cu wire, are wound around a cylinder of thin Mylar sheet, with the sample inside the cylinder, and then placed inside a piston–clamp type Cu–Be high pressure cell with Daphne oil as the pressure transmitting medium. The pressure so generated is hydrostatic. The pressure at low temperatures was determined from the superconducting transition of a small (∼1 mg) piece of lead Pb which was loaded in the cell with the sample.

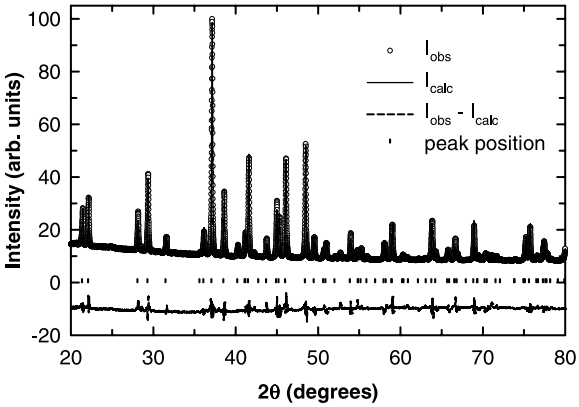

Figure 1. Rietveld refinement of the $Tm_2Fe_3Si_5$ powder x-ray diffraction data. The open symbols represent the observed data, the solid lines through the data represent the fitted pattern, the dotted lines represent the difference between the observed and calculated intensities and the vertical bars represent the peak positions.

3. Results

3.1. Crystal growth and structure

The tantalum container was cut open using a saw and the Al_2O_3 crucible removed. Inside this crucible one could see a melted mass of material stuck to the crucible walls. The Al_2O_3 crucible was cut off from the bottom and the sides using a diamond-wheel cutter. The cutting was done carefully to minimize the loss of material. The melted ingot was then lightly tapped from the sides with a hammer and crystals in the form of platelets with a largest size of 1.25 × 1 × 0.25 mm^3 physically extracted. Some of the smaller crystals were crushed for powder x-ray diffraction (XRD) study. Cobalt radiation (Co Kα) was used to suppress the fluorescence from the Fe. The XRD of the crushed crystals (shown in figure 1) confirmed the structure and absence of impurity phases and sharp Laue back-scattering patterns indicated that the crystals were of high quality. All the peaks in the powder XRD pattern could be indexed to the known $Sc_2Fe_3Si_5$ type structure (space group $P4/mnc$), and a Rietveld refinement, shown as the solid curve through the data in figure 1, gave the lattice constants $a = b = 10.371(3)$ Å and $c = 5.403(5)$ Å which are in good agreement with the literature values ($a = b = 10.367$ Å

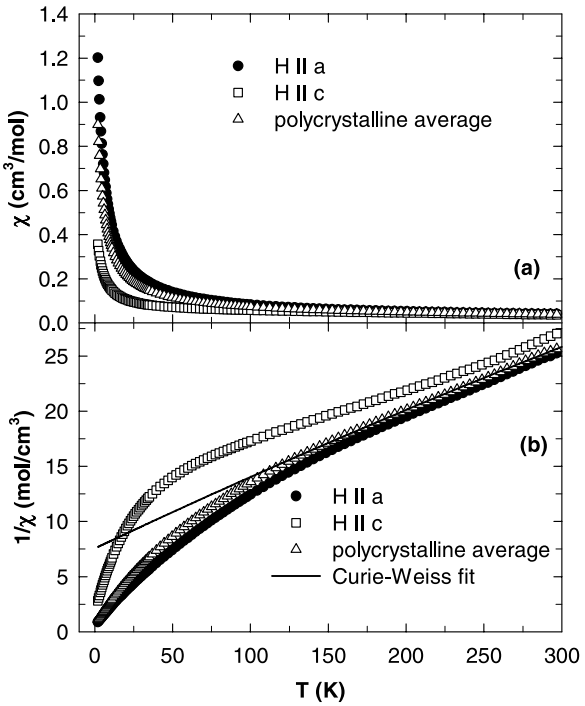

Figure 2. (a) Temperature T dependence of the static magnetic susceptibility χ of $Tm_2Fe_3Si_5$ from 1.8 to 300 K in a field of 1 kOe applied along the a and c axes. The polycrystalline average susceptibility is also shown. (b) Temperature T dependence of the inverse susceptibility $(1/\chi)$. The solid line is a fit to the Curie–Weiss relation (see the text).

and $c = 5.407$ Å) [16]. From Laue back-scattering pictures the largest surfaces of the plate-like crystals were found to be perpendicular to either the a axis or the b axis. The Laue measurements were also used to find the (001) orientation (the tetragonal c axis) of the crystals.

3.2. Ambient pressure measurements

3.2.1. Magnetic susceptibility. In figure 2 we present the results of the anisotropic static susceptibility χ measurements. Figure 2(a) shows the $\chi(T)$ data between 1.8 and 300 K in a field of 1 kOe applied along the a and c axes. As expected for a tetragonal system, the susceptibilities along the a and b axes (not shown) are the same. The polycrystalline averaged susceptibility χ_{poly} which can be calculated as

$$\chi_{poly}(T) = \frac{\chi_a(T) + \chi_b(T) + \chi_c(T)}{3} \qquad (1)$$

is also shown.

The susceptibility is moderately anisotropic with the easy axis of magnetization being perpendicular to the tetragonal c axis and $\chi_a/\chi_c = 3.2$ at 1.8 K. Within a series of isostructural rare-earth based compounds, the magnetocrystalline anisotropy changes from uniaxial (easy axis along c axis) to easy plane (easy axis perpendicular to c axis) behavior at Er [17]. These systematics have been observed in $\chi(T)$ measurements on oriented polycrystals of other magnetic members (R = Gd–Er) of this series [2]. The results for $Tm_2Fe_3Si_5$, therefore, follow the expected trend.

The plots of the inverse susceptibilities are shown in figure 2(b). The $1/\chi_c$ data in figure 2(b) show a curvature over the whole temperature range with a broad minimum at about 250 K and could not be fitted with a Curie–Weiss expression. The $1/\chi_a$ data between 130 and 300 K could be fitted with a modified Curie–Weiss expression given by

$$\chi = \chi_0 + \frac{C}{(T-\theta)}. \qquad (2)$$

The fit (not shown here) gave the values $\chi_0 = 4.3(8) \times 10^{-3}$ cm^3 Tm^{-1} mol^{-1}, $C = 7.0(3)$ cm^3 Tm^{-1} mol^{-1}K^{-1}, and $\theta = -88(5)$ K. The value $C = 7.0(3)$ cm^3 Tm^{-1} mol^{-1} K^{-1} corresponds to an effective moment of $\mu_{eff} = 7.5(2)\ \mu_B$ which is close to the free moment value 7.56 μ_B for trivalent Tm moments. However, fitting the $1/\chi_a(T)$ data between 300 K and some temperature T^* above 130 K gave θ and C values which depended on T^*. For example, with $T^* = 200$ K, the fit gave $\chi_0 = 3.9(5) \times 10^{-3}$ cm^3 Tm^{-1} mol^{-1}, $C = 6.7(1)$ cm^3 Tm^{-1} mol^{-1} K^{-1}, and $\theta = -65(3)$ K. The $1/\chi_{poly}(T)$ data between 150 and 300 K could also be fitted with equation (2). The fit, shown as the solid line extrapolated to $T = 0$ K, in figure 2(b), gave the values $\chi_0 = 4.0(4) \times 10^{-3}$ cm^3 Tm^{-1} mol^{-1}, $C = 6.9(3)$ cm^3 Tm^{-1} mol^{-1} K^{-1}, and $\theta = -109(6)$ K. The value $C = 6.9(3)$ cm^3 Tm^{-1} mol^{-1} K^{-1} corresponds to an effective moment of $\mu_{eff} = 7.4(4)\ \mu_B$. The dependence of the fitting parameters on the temperature range of the fit was also found for the χ_{poly} data.

To the best of our knowledge there is only one previous report of the static magnetic susceptibility of a polycrystalline sample of this material [16]. It was reported in [16] that the magnetic susceptibility data between 70 and 300 K could be fitted with a Curie–Weiss law plus a constant term with an effective moment 7.0(3) μ_B. The value of θ was not reported, and the effect of changing the temperature range of the fit was not discussed. Comparing our $1/\chi(T)$ data in figure 2(b) to those for the polycrystalline sample in figure 7 of [16] it is clear that the polycrystalline sample must have had a large preferential orientation along the c axis. A definite curvature in the $1/\chi(T)$ data at high temperatures for the polycrystalline sample in figure 7 of [16] can be seen.

The large value of θ compared to the magnetic ordering temperature (discussed below) and the temperature dependence of the $\chi(T)$ data above are interesting and we will return to these in section 4 below when we discuss our results.

Figure 3 shows the ambient pressure ac susceptibility χ_{ac} data between 0.1 and 4 K in zero applied dc magnetic field. The peak in χ_{ac} at $T_N = 1.15$ K indicates the onset of antiferromagnetic ordering. The shape of the anomaly at T_N is unusual and different from what is usually observed at an antiferromagnetic transition. The sharp drop in χ_{ac} by more than 10% and the weak temperature dependence at lower temperatures suggests the presence of a spin gap in this system below T_N. We can estimate the value of the spin gap by fitting the data below the magnetic transition using the following expression:

$$\chi = \chi_0 + a \exp^{-\Delta/k_B T}, \qquad (3)$$

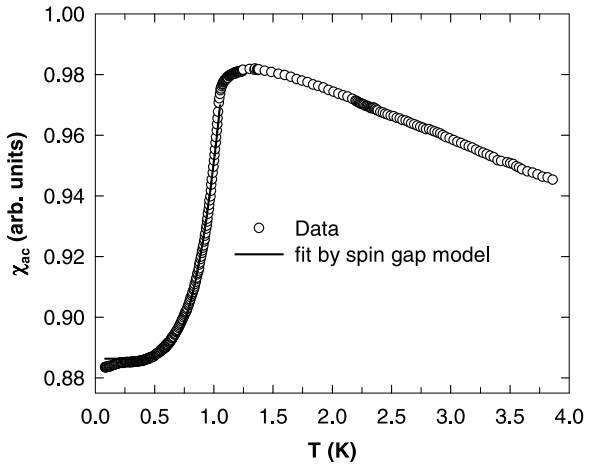

Figure 3. Temperature dependence of the zero-field ac susceptibility χ_{ac} of $Tm_2Fe_3Si_5$ from 100 mK to 4 K. The sharp anomaly peaked around 1.15 K is the signature of antiferromagnetic ordering. The solid curve through the data is a fit with equation (3).

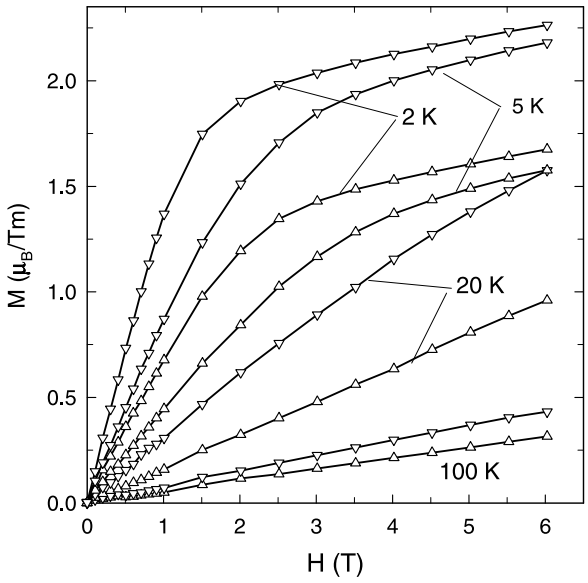

Figure 4. Anisotropic isothermal magnetization M of $Tm_2Fe_3Si_5$ versus magnetic field H at various temperatures, with H along the a axis (▽) and c axis (△).

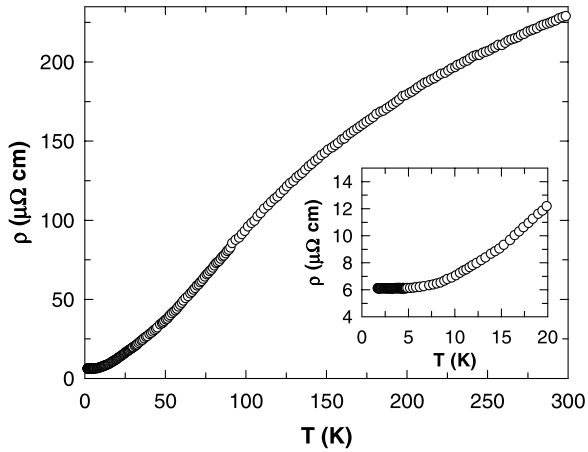

Figure 5. Resistivity ρ versus temperatures T of $Tm_2Fe_3Si_5$ with current I along the a axis.

and the fit, shown as the solid curve through the data, gave the gap value $\Delta = 2.4(2)$ K. We observe a small bump in χ_{ac} below 0.25 K, the origin of which is not clear at present. We did not observe any signature of superconductivity down to 0.1 K.

3.2.2. Magnetization. The magnetization M versus field H at various temperatures T is shown in figure 4. At high temperatures the M data are linear with applied field and the anisotropy between the a and c axis magnetization is small. The $M(H)$ data begin to show a curvature below 20 K and in the data for 5 and 2 K it can clearly be seen that the anisotropy between the a and c axes is larger and there is a tendency of saturation on increasing the field. The magnetization, however, continues to increase with field up to the highest applied field, $H = 6$ T. The expected saturation magnetization for a magnetic ion is given by $M_{sat} = g_J J$, where g_J is the Landé g-factor and J is the total angular momentum. For trivalent Tm, $g_J = \frac{7}{6}$ and $J = 6$ giving $M_{sat} = 7\ \mu_B$. The magnetization at 2 K at the highest field 6 T is much smaller, most likely due to the fact that the ground state is a quasi-doublet. The curvature in M at temperatures above T_N probably indicates strong magnetic correlations as one approaches T_N.

3.2.3. Resistivity. The resistivity $\rho(T)$ of $Tm_2Fe_3Si_5$ between 1.5 and 300 K for excitation current $I = 5$ mA along the a axis is shown in the main panel of figure 5. The sample exhibits normal metallic behavior with a room temperature value $\rho(300\ \text{K}) = 233\ \mu\Omega$ cm and a monotonic decrease with T. The inset shows the low temperature data between 1.5 and 20 K on an expanded scale. The small value of the residual resistivity $\rho(1.5\ \text{K}) = 6\ \mu\Omega$ cm and a reasonably large residual resistivity ratio RRR $= \rho(300\ \text{K})/\rho(1.5\ \text{K}) = 39$ indicates good sample quality. We did not observe any signature of superconductivity down to 1.5 K in our resistivity measurements. The temperature dependence of ρ is qualitatively similar to the only other resistance measurement that was reported for a polycrystalline sample which showed a partial superconducting transition below 1.8 K at ambient pressure [10]. The reported residual resistivity ratio was about 40 which is close to what we observe for our single-crystal sample.

3.2.4. Heat capacity. The temperature dependence of the heat capacity C of $Tm_2Fe_3Si_5$ between 0.3 and 35 K is shown in figure 6(a). The sharp peak of nearly 20 J Tm^{-1} mol^{-1} K^{-1} just above $T_N = 1$ K confirms the bulk antiferromagnetic ordering in this compound. To estimate the magnetic contribution to C we tried to use the heat capacity $C_{Lu_2Fe_3Si_5}$ of the isostructural non-magnetic compound $Lu_2Fe_3Si_5$. The $C_{Lu_2Fe_3Si_5}$ data set, shown in figure 6(a), was taken from our previous paper on $Yb_2Fe_3Si_5$ [7]. The difference ΔC between C and $C_{Lu_2Fe_3Si_5}$ is also shown in figure 6(a). $C_{Lu_2Fe_3Si_5}$ is larger than C above $T = 28$ K which gives an unphysical negative ΔC as seen in figure 6(a). This indicates that the

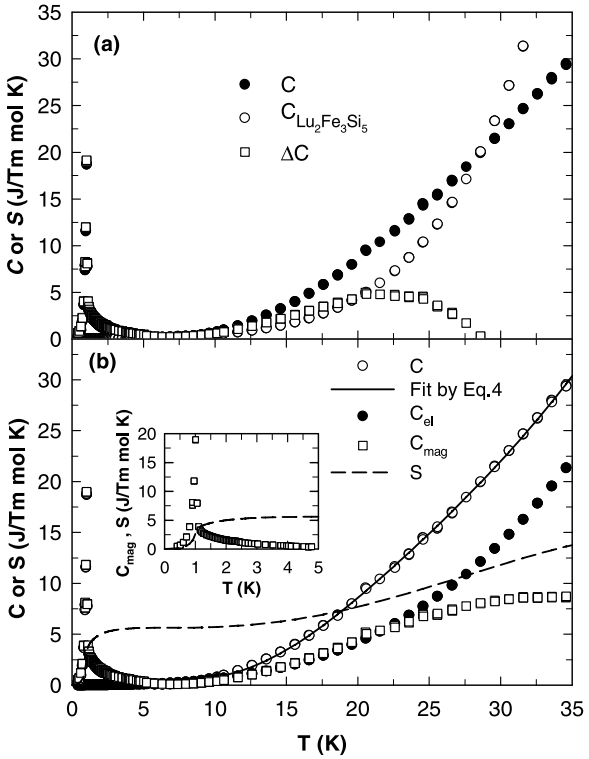

Figure 6. (a) The heat capacity C versus temperature T for $Tm_2Fe_3Si_5$ from 0.3 to 35 K. Also shown are the heat capacity of $Lu_2Fe_3Si_5$, $C_{Lu_2Fe_3Si_5}$, and the difference ΔC between C and $C_{Lu_2Fe_3Si_5}$. (b) The heat capacity C versus T, the fit with equation (4), the magnetic heat capacity C_{mag}, and the entropy S versus T. The inset in (b) shows the low temperature C_{mag} and S data between 0.3 and 5 K.

lattice dynamics of the two materials are probably different and that $C_{Lu_2Fe_3Si_5}$ is not an appropriate estimation of the lattice heat capacity for $Tm_2Fe_3Si_5$. The $\Delta C(T)$ data set in figure 6(a) suggests that there is a contribution to the C from a Schottky-like anomaly above 20 K. To estimate the electronic C_{el}, lattice C_{ph} and Schottky $C_{Schottky}$ contributions to C we fitted the $C(T)$ data between 10 and 35 K using the expression [18]

$$C = C_{el} + C_{ph} + C_{Schottky} = \gamma T + \beta T^3 + \frac{g_0}{g_1}\left(\frac{\delta}{T}\right)^2 \frac{\exp(\frac{\delta}{T})}{\left[1 + \frac{g_0}{g_1}\exp(\frac{\delta}{T})\right]^2}, \quad (4)$$

where γ is the Sommerfeld coefficient, δ is the energy splitting between a ground state of degeneracy g_0 and an excited state of degeneracy g_1. The fit, shown as the solid curve through the $C(T)$ data in figure 6(b), gave the values $\gamma = 56(4)$ mJ Tm^{-1} mol^{-1} K^{-2}, $\beta = 0.94(4)$ mJ Tm^{-1}mol^{-1} K^{-4}, $g_0/g_1 = 0.329(3)$, and $\delta = 98(3)$ K. From the value of β one can estimate the Debye temperature θ_D using the expression [18]

$$\Theta_D = \left(\frac{12\pi^4 Rn}{5\beta}\right)^{1/3}, \quad (5)$$

where R is the molar gas constant and n is the number of atoms per formula unit ($n = 10$ for $Tm_2Fe_3Si_5$). We obtain $\theta_D = 268(8)$ K.

The magnetic contribution C_{mag} which was obtained by subtracting C_{el} and C_{ph} from C, and the estimated entropy S obtained by integrating the C_{mag}/T versus T data are also shown in figure 6(b). The inset in figure 6(b) shows C_{mag} and S between 0.3 and 5 K to highlight the low temperature behavior. The entropy reaches a value of 4.53 J Tm^{-1} mol^{-1} K^{-1} at T_N which is smaller than the value $R \ln 2 = 5.76$ J Tm^{-1} mol^{-1} K^{-1} expected for a doublet ground state. An entropy of $R \ln 2$ is reached only near 5 K after which the entropy increases only weakly up to about 10 K. The tail in $C(T)$ above T_N and the weak temperature dependence of S between 5 and 10 K strongly indicate that the ground state is a quasi-doublet with a small splitting due to the crystalline electric field (CEF). For higher temperature the entropy increases again, probably due to contributions from a Schottky-like anomaly as indicated in the $C_{mag}(T)$ data in figure 6(b). The value of δ obtained above indicates that the first excited CEF level is about 100 K above the quasi-doublet ground state. This value is consistent with the fact that the $\chi(T)$ data deviate from the Curie–Weiss law below about 130 K.

At 35 K the entropy reaches a value of about 13 J Tm^{-1} mol^{-1} K^{-1} which is much smaller compared to the full $R \ln(2J+1)$ ($\approx$22 J Tm^{-1} mol^{-1} K^{-1}) expected for Tm^{3+} ($J = 6$) moments. Considerably higher temperatures need to be attained to observe the full entropy.

3.3. High pressure ac susceptibility

The temperature dependence of the ac susceptibility $\chi_{ac}(T)$ of $Tm_2Fe_3Si_5$ was measured between 1.8 and 10 K with various applied pressures P. The $\chi_{ac}(T)$ data for $P = 3.5$, 5, and 8.5 kbar are shown in figure 7. The superconducting transition for a small piece of lead Pb loaded along with the sample is indicated by the arrow in the figure. There is no superconducting transition at ambient pressure (see figure 3). We observe the onset of a superconducting transition below 1.9 K only at a pressure of about 2 kbar (not shown). For higher pressures the superconducting transition temperature increases and a full transition is observed for $P = 8.5$ kbar. We estimate a superconducting volume fraction of 125% at $T = 2$ K for the data at $P = 8.5$ kbar without correcting for demagnetization factors.

The temperature T versus pressure P phase diagram for $Tm_2Fe_3Si_5$ is shown in figure 8. The non-linear dependence of T_c on pressure P with a maximum at around 8.5 kbar is similar to the behavior reported for polycrystalline samples which do not show a superconducting transition at ambient pressure [16]. The initial pressure coefficient dT_c/dP for our single-crystalline sample was determined as about 0.22 K kbar^{-1}.

4. Discussion

In previous reports the magnetic susceptibility at the antiferromagnetic transition was obscured by the fact that it occurs very close to the superconducting transition. We have shown by means of measurements on the stoichiometric

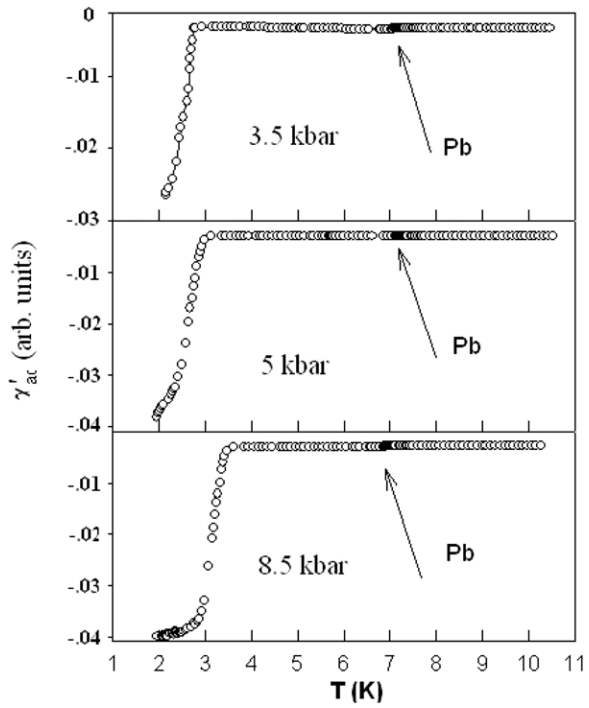

Figure 7. Temperature T dependence of the ac susceptibility χ_{ac} of $Tm_2Fe_3Si_5$ under various pressures P. P was determined from the superconducting transition of lead (Pb) indicated by the arrow.

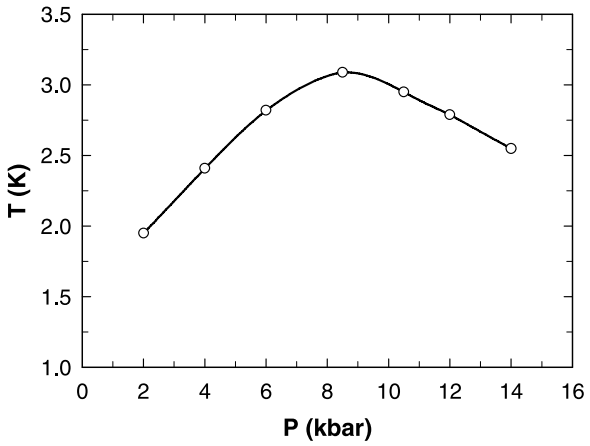

Figure 8. Temperature T versus pressure P phase diagram of $Tm_2Fe_3Si_5$ showing the pressure dependence of the superconducting transition temperature. The line through the data is a guide to the eye.

material that at T_N the shape of χ_{ac} is unusual and it shows a sudden decrease below the transition before leveling off at a finite value at the lowest temperatures. The sudden drop in χ below the transition and a finite non-zero susceptibility at the lowest temperatures probably indicate partial gapping of the Fermi surface below T_N. A spin gap could occur if the magnetic order below T_N is accompanied by a spin density wave (SDW). Neutron diffraction measurements, preferably on a stoichiometric sample of $Tm_2Fe_3Si_5$, will be needed to check this possibility. Resistivity measurements on a stoichiometric sample down to temperatures below T_N would also be useful to look for signatures of partial gapping of the Fermi surface below T_N.

The values of $\theta \sim -90$ K, obtained by fitting the χ_a or the χ_{poly} data are unusually large considering that antiferromagnetic ordering occurs at 1.1 K in this compound. A large θ and a comparatively much smaller ordering temperature is sometimes seen in systems where the magnetic interactions are frustrated. The crystal structure of $Tm_2Fe_3Si_5$ does not suggest this possibility. Another class of systems where a large θ is seen are the systems with valence fluctuations [19]. Indeed the temperature dependence of the $\chi_c(T)$ data is similar to what is observed for valence fluctuating materials. The dependence of the values of the effective moment and the Weiss temperature on the temperature range of the Curie–Weiss fit is also what has been theoretically predicted for valence fluctuating Tm compounds [20]. Valence fluctuations and hybridization between the 4f and conduction electrons are also supported by the moderately enhanced $\gamma = 56(4)$ mJ Tm^{-1} mol^{-1} K^{-2} in the paramagnetic state. Valence fluctuations are known to suppress superconductivity, and the application of pressure, which will stabilize the Tm^{3+} state and suppress the valence fluctuations, will therefore enhance the superconductivity. This is exactly what is observed for $Tm_2Fe_3Si_5$. Our data therefore suggest that valence fluctuations of Tm moments and/or the partial gapping of the Fermi surface below T_N could be possible mechanisms for the destruction of superconductivity in $Tm_2Fe_3Si_5$.

5. Conclusion

We have grown high quality, stoichiometric single crystals of the compound $Tm_2Fe_3Si_5$ using a modified Bridgman method and characterized them using x-ray, Laue back-scattering, $\chi(T)$, $M(H)$, $\chi_{ac}(T)$, $\rho(T)$, $C(T)$ and high pressure $\chi_{ac}(T)$ measurements. Anomalies in the ambient pressure $\chi_{ac}(T)$ and $C(T)$ confirm bulk antiferromagnetic ordering at $T_N = 1.1$ K in this compound. The χ_{ac} drops abruptly below T_N suggesting a partial gapping of the Fermi surface. The $\chi_c(T)$ data and the analysis of the χ_a and χ_{poly} data and the enhanced $\gamma = 56(4)$ mJ Tm^{-1} mol^{-1} K^{-2} in the paramagnetic state point to the possibility of valence fluctuations in this material. These results suggest that valence fluctuations and/or gapping of the Fermi surface below T_N are possible mechanisms for the destruction of superconductivity in $Tm_2Fe_3Si_5$.

Acknowledgments

YS would like to thank C Geibel for useful discussions about the crystal growth and the Max Planck Institute for the Chemical Physics of Solids, Dresden, for support during his visit in 2000–2001.

References

[1] Braun H F 1980 *Phys. Lett.* A **75** 386
[2] Braun H F, Segre C U, Acker F, Rosenberg M, Dey S and Deppe P 1981 *J. Magn. Magn. Mater.* **25** 117

[3] Moodenbaugh A R, Cox D E and Braun H F 1982 *Phys. Rev.* B **25** 4702
[4] Vining C B 1983 *Report* IS-T-1053; Order No. DE83016130
[5] Vining C B and Shelton R N 1983 *Phys. Rev.* B **28** 2732
[6] Vining C B, Shelton R N, Braun H F and Pelizzone M 1983 *Phys. Rev.* B **27** 2800
[7] Singh Y, Ramakrishnan S, Hossain Z and Geibel C 2002 *Phys. Rev.* B **66** 014415
[8] Cashion J D, Shenoy G K, Niarchos D, Viccaro P J and Falco C M 1980 *Phys. Lett.* A **79** 454
[9] Cashion J D, Shenoy G K, Niarchos D, Viccaro P J, Aldred A T and Falco C M 1981 *J. Appl. Phys.* **52** 2180
[10] Segre C U and Braun H F 1981 *Phys. Lett.* A **85** 372
[11] Moodenbaugh A R, Cox D E and Vining C B 1985 *Phys. Rev.* B **32** 3103
[12] Vining C B and Shelton R N 1985 *Solid State Commun.* **54** 53
[13] Gotaas J A, Lynn J W, Shelton R N, Klavins P and Braun H F 1987 *Phys. Rev.* B **36** 7277
[14] Grigereit T E, Lynn J W, Huang Q, Santoro A, Cava R J, Krajewski J J and Peck W F Jr 1994 *Phys. Rev. Lett.* **73** 2756
[15] Fertig W A, Johnston D C, Delong L E, McCallum R W, Maple M B and Matthias B T 1977 *Phys. Rev. Lett.* **38** 987
[16] Schmidt H, Muller M and Braun H F 1996 *Phys. Rev.* B **53** 12389
[17] See e.g. Buschow K H J and de Boer F P 2003 *Physics of Magnetism and Magnetic Materials* (Dordrecht: Kluwer Academic/Plenum)
[18] Kittel C 1966 *Solid State Physics* (New York: Wiley)
[19] Batlogg B, Ott H R, Kaldis E, Thoni W and Wachter P 1979 *Phys. Rev.* B **19** 247
[20] Aligia A A and Alascio B 1984 *J. Magn. Magn. Mater.* **43** 119